Mechanical Properties of β-Catenin Revealed by Single-Molecule Experiments

Alejandro Valbuena,[†] Andrés Manuel Vera,[†] Javier Oroz,[†] Margarita Menéndez,[‡] and Mariano Carrión-Vázquez[†]

[†]Instituto Cajal/CSIC, Centro de Investigación Biomédica en Red sobre Enfermedades Neurodegenerativas (CIBERNED) and IMDEA Nanociencia, Madrid, Spain; and [‡]Instituto de Química-Física Rocasolano, CSIC and Centro de Investigación Biomédica en Red sobre Enfermedades Respiratorias (CIBERES), Madrid, Spain

SUPPORTING MATERIAL

SUPPORTING METHODS

Protein engineering

Full-length β-catenin

The His-tagged β-catenin (UniProt KB/Swiss-Prot code P35222, **Fig. 1 *C***) cloned (S1) in the pQE32 plasmid (Stratagene, La Jolla, CA) was expressed in the BL21(DE3) *E. coli* strain (Novagen, Madison, WI). Cells were grown at 37 ºC to an OD_{595} of ~ 0.5 and expression was then induced by 1mM Isopropyl β-D- thiogalactopiranoside (IPTG) for 3 h. The protein was purified by Ni^{2+}-affinity chromatography using Histrap HP FPLC columns (GE Healthcare Bio-Science AB, Uppsala, Sweden). Proteins were bound in 50 mM phosphate buffer (NaP)/500 mM NaCl/50 mM imidazole, pH 7.4, and they were eluted with 50 mM NaP/500 mM NaCl/500 mM imidazole, pH 7.4. After affinity purification, anionic exchange chromatography was performed using HiTrap Q columns (GE Healthcare) in 50 mM NaP/50 mM NaCl/1 mM DTT/1 mM EDTA, pH 7.4, by increasing the ionic strength lineally to 1 M NaCl. Fractions containing full-length β-catenin were pooled and further purified by size exclusion chromatography in a Hiload 16/60 column (GE Healthcare) in 50 mM NaP/300 mM NaCl/1mM EDTA/1 mM DTT. The protein was concentrated by ultrafiltration using Amicon 10K filters (Millipore, Billerica, MA) and then dialysed by Spectra/Por Dialysis Membrane 3 (Spectrum Laboratories, Rancho Dominguez, CA) in either PBS/0.2 mM EDTA/5mM DTT buffer for AFM experiments or PBS/0.2 mM EDTA/1mM DTT for circular dichroism (CD) experiments. Purity of the protein was estimated to be higher that 95% from Coomassie-stained polyacrylamide gel electrophoresis (PAGE).

Cloning and expression of hetero-polyproteins

The ARM repeats region from human β-catenin (amino acids 134-671) was cloned in the pRSETA-$(I27)_8$ vector fused to flanking I27 domains (**Fig. 1 *C***), used as single-molecule markers (23). The restriction sites used for cloning were KpnI and MluI and the template used for β-catenin PCR-amplification was a pQE32 plasmid (Qiagen Gmbh, Hilden, Germany) containing the full-length His-tagged β-catenin (S1). Cloning of human full-length β-catenin into the previous vector was done using the restriction sites KpnI and MluI and the template mentioned before for PCR amplification. Cloning steps were carried out in the XL1Blue *E. coli* strain (Stratagene). The sequences of both constructs, $(I27)_3$-β-$catenin_{full\text{-}length}$-I27 and $(I27)_3$-β-$catenin_{ARM}$-I27 (βI27 and ARMI27, as termed in the text), were verified by sequencing both strands of the cloned β-catenin.

Proteins were expressed in the BLR (DE3) *E. coli* strain (Novagen) and cells grown at 37 ºC to an OD_{595} of ~ 0.5. Expression was induced by adding 1mM IPTG overnight at room temperature, in the case of βI27, and for 3 h at 37 ºC for ARMI27. Proteins were purified by Ni^{2+}-affinity chromatography using Histrap HP FPLC columns (GE Healthcare Bioscience AB) using the aforementioned buffers. The purification strategy included an additional step of size-exclusion chromatography on a Hiload 16/60 column (GE Healthcare) in 100 mM NaP/100 mM NaCl/1mM DTT/1mM EDTA, pH 7. Purified fractions were concentrated and the buffer was exchanged to PBS/0.2 mM EDTA/5mM DTT, pH 7.4, by ultrafiltration using Amicon 10K filters (Millipore). ARMI27 was also dialysed directly after the Ni^{2+}-affinity chromatography (Spectra/Por Dialysis Membrane 3) against PBS/0.2 mM EDTA/5mM DTT buffer for AFM experiments and in PBS/0.2 mM EDTA/1mM DTT for CD experiments. The final protein concentration was kept at 0.3-0.4 mg/ml, as measured by their OD_{280} using their extinction coefficients. Protein purity was estimated to be higher that 95 % from Coomassie-stained PAGE.

I27 polyprotein

As a CD control for secondary structure, we have used $(I27)_8$ polyprotein (24) which was expressed in the C41 (DE3) strain (S2). Cells were grown at 37 ºC to an OD_{595} of ~ 0.7 and then expression was induced by 1 mM IPTG for 4 h at 37 ºC. Recombinant proteins were purified by Ni^{2+}-affinity chromatography with Histrap HP FPLC columns (GE Healthcare) as mentioned. Proteins were then subjected to size-exclusion chromatography in a Hiload 16/60 column (GE Healthcare) using as buffer 50 mM NaP/300 mM NaCl/1mM EDTA/1 mM DTT, pH 7.4. Purified fractions were concentrated by ultrafiltration with Amicon filters (10K Millipore) and then dialysed (Spectra/Por Dialysis Membrane 3) against PBS/0.2 mM EDTA/1mM DTT. The final protein concentration was ~1mg/ml. Protein purity was estimated to be higher that 95 % from Coomassie-stained PAGE.

Gold-coated coverslips

We performed some AFM experiments on gold-coated coverslips because our ARM construct has two terminal cysteine residues, which can covalently bind to gold surfaces (S3). We cleaned glass coverslips by sonication in 15 min steps, first with EtOH, then with 0.1 % Helmanex II (Hellma GmbH & Co. KG, Mülheim, Germany) and, finally, with deionized water (MilliQ, 18 MΩ·cm, 0.22 μm filtered). Between each sonication step, the coverslips were rinsed profusely with MilliQ water. The coverslips were then dried under a N_2 flow and placed in a custom made vacuum chamber (at ~ $2 \cdot 10^{-6}$ mbar). Then, by thermal evaporation, an adhesive layer of chromium was deposited followed by a final gold layer.

NTA-Ni^{2+} coverslips functionalization.

Our recombinant polyproteins contained an N-terminal Histag which can bind to NTA-Ni^{2+} functionalized surfaces (S4). Coverslips were first immersed into a 20 N KOH solution overnight. Then they were placed under a MilliQ water flow for 1 h before being transferred to a 2 % 3-(mercaptopropyl)triethoxysilane (Sigma-Aldrich, San Louis, MO), 0.02 % acetic acid at 90ºC for 1 h. Afterwards, they were washed in MilliQ water flow for 1 h and then cured for 15 min in an oven at 120ºC. Next they were transferred to a 100 mM DTT solution for 15 min and washed under a MilliQ water flow for 1 h. Then, a solution of 20 mg/ml maleimide-C_3-NTA (Dojindo Laboratories, Kumamoto, Japan) dissolved in 10 mM 3-(N-morpholino)propanesulfonic acid (pH 7) was added (50 μl) and incubated for 1/2 h. After a final wash in MilliQ water, a drop of 10 mM $NiCl_2$ was added (> 50 μl) on the coverslips, incubating for 10 min, and they were washed with MilliQ water before storage.

Circular dichroism of proteins

Far-UV CD spectra of the polyproteins and their isolated components were acquired in PBS/0.2 mM EDTA/1 mM DTT, pH 7.4, in a JASCO-J810 spectropolarimeter (JASCO Inc., Tokyo, Japan), as described previously (S5). After correction for the buffer contribution, the experimental data were converted to molar ellipticities (Θ) using as average molecular masses per residue: 110.11 $(I27)_8$, 109.65 (β-catenin and ARMI27) and 109.72 (βI27). The content in secondary structure of each construct was estimated by spectra deconvolution using the CDNN program (S6). Thermal denaturation was followed by measuring the ellipticity changes induced by the temperature increase (60ºC/h) at fixed wavelengths.

SUPPORTING RESULTS

Secondary structure controls

In order to exclude the possibility that the I27 modules may have induced secondary structural changes in the ARM region in the fusion proteins, we also performed structural studies by CD. The far-UV spectrum of ARMI27 exhibited the characteristic features of α-helical structures (**Fig. S11 *A***) and the values estimated (40 % α-helix and 15 % β-structure) by spectrum deconvolution are consistent with those expected considering the tridimensional structures of β-catenin and I27 (13, S7). Furthermore, we showed that thermal denaturation of the ARMI27 displayed a biphasic profile (**Fig. S11 *B***); the first phase ($T^1_{1/2}$ = 55.9ºC) overlapped with the denaturation interval of full-length β-catenin ($T_{1/2}$ = 56.1ºC), while the second one ($T^2_{1/2}$ = 65.4ºC) took place in the same range as thermal transitions of $(I27)_8$ ($T_{1/2}$ = 69.2ºC) and I27 ($T_{1/2}$ = 68.3ºC) (at $T_{1/2}$ 50% of protein is native and 50% unfolded). Similar results were found for βI27 ($T^1_{1/2}$ = 55.7 ºC, $T^2_{1/2}$ = 67.8 ºC). Besides, the denaturation profiles of the three constructs containing the ARM region showed narrow cooperative transitions.

SUPPORTING REFERENCES

S1. Behrens, J., J. P. von Kries, M. Kühl, L. Bruhn, D. Wedlich, R. Grosschedl, and W. Birchmeier. 1996. Functional interaction of β-catenin with the transcription factor Lef-1. *Nature.* 382:638-642.

S2. Miroux, B., and J. Walker. 1996. Over-production of proteins in Escherichia coli: mutant hosts that allow synthesis of some membrane proteins and globular proteins at high levels. *J. Mol. Biol.* 260:289-298.

S3. Rief, M., M. Gautel, F. Oesterhelt, J. M. Fernández, and H. E. Gaub. 1997. Reversible unfolding of individual titin immunoglobulin domains by AFM. *Science.* 276:1109-1112.

S4. Hossain M.D., S. Furuike, Y. Maki, K. Adachi, M.Y. Ali, M. Huq, H. Itoh, M. Yoshida and K. Kinosita Jr. 2006. The rotor tip inside a bearing of a thermophilic F1-ATPase is dispensable for torque generation. *Biophys. J.* 90:4195-4203.

S5. Varea, J., B. Monterroso, J. Sáiz, C. López-Zumel, J. García, J. Laynez, P. García, and M. Menéndez. 2004. Structural and thermodynamic characterization of Pal, a phage natural chimeric lysin active against pneumococci. *J. Biol. Chem.* 279:43697-43707.

S6. Böhm, G., R. Muhr, and R. Jaenicke. 1992. Quantitative analysis of protein far UV circular dichroism spectra by neural networks. *Prot. Eng.* 5:191-195.

S7. Improta, S., A. Politou, and A. Pastore. 1996. Immunoglobulin-like modules from titin I-band: extensible components of muscle elasticity. *Structure.* 4:323-337.

S8. Zinober, R. C., D. J. Brockwell, G. S. Beddard, A. W. Blake, P. D. Olmsted, S. E. Radford, and D. A. Smith. 2002. Mechanically unfolding proteins: The effect of unfolding history and the supramolecular scaffold. *Prot. Sci.* 11: 2759-2765.

S9. Evans, E., and K. Ritchie.1999. Strength of a weak bond connecting flexible polymer chains. *Biophys. J.* 76: 2439-2447.

SUPPORTING FIGURES

FIGURE S1

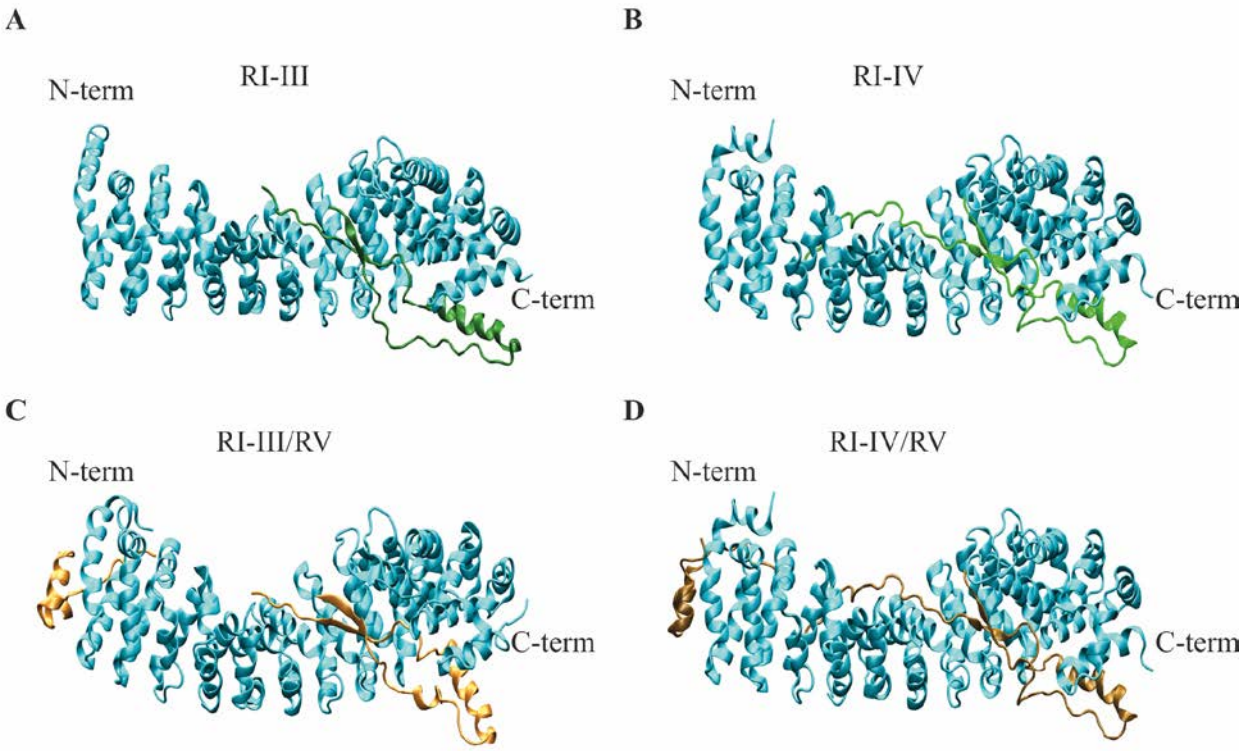

FIGURE S2

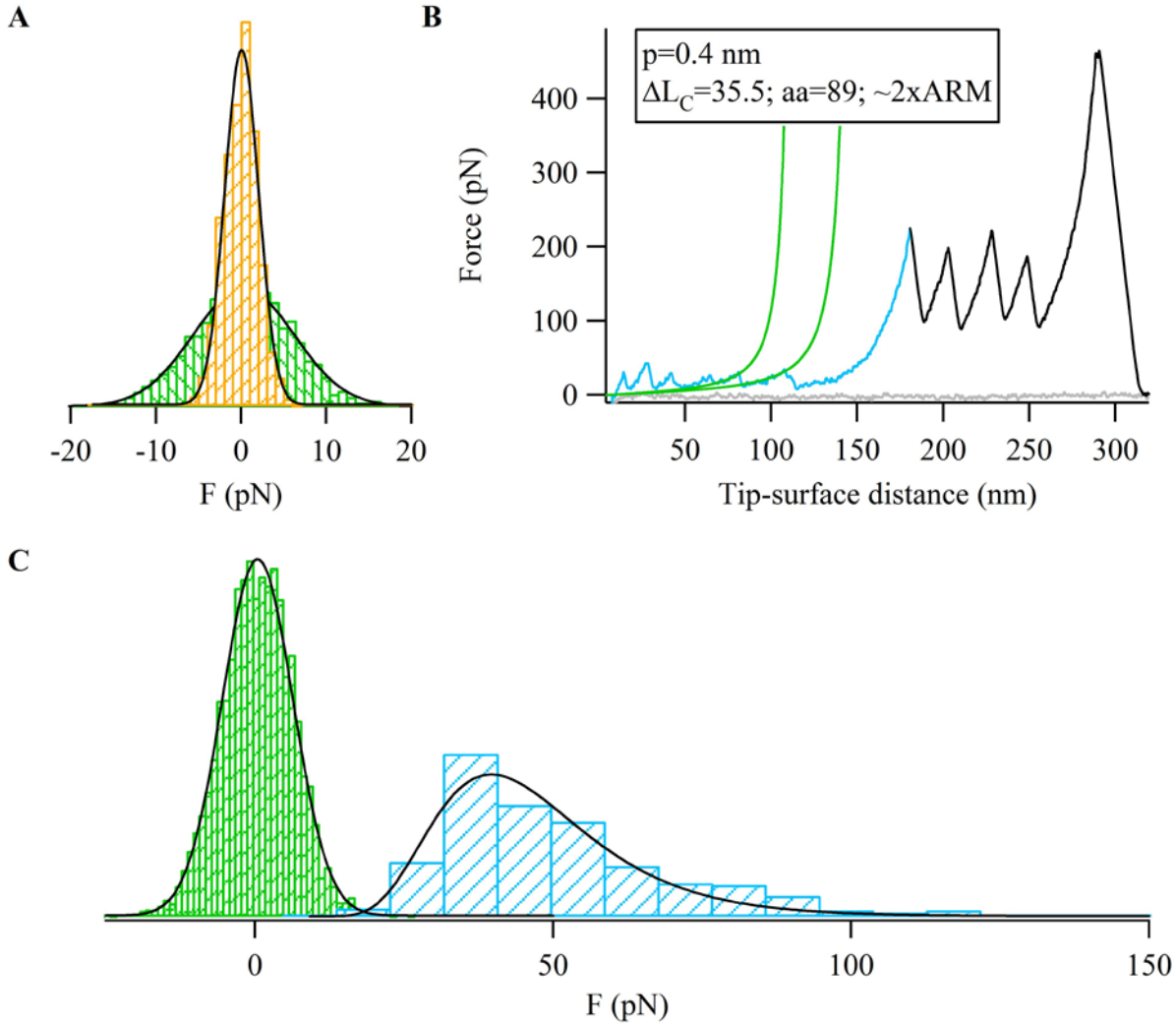
A
-20
-10
0
10
20
F (pN)
B
p=0.4 nm
ΔL_C=35.5; aa=89; ~2xARM
Force (pN)
400
300
200
100
0
50
100
150
200
250
300
Tip-surface distance (nm)
C
0
50
100
150
F (pN)

FIGURE S3

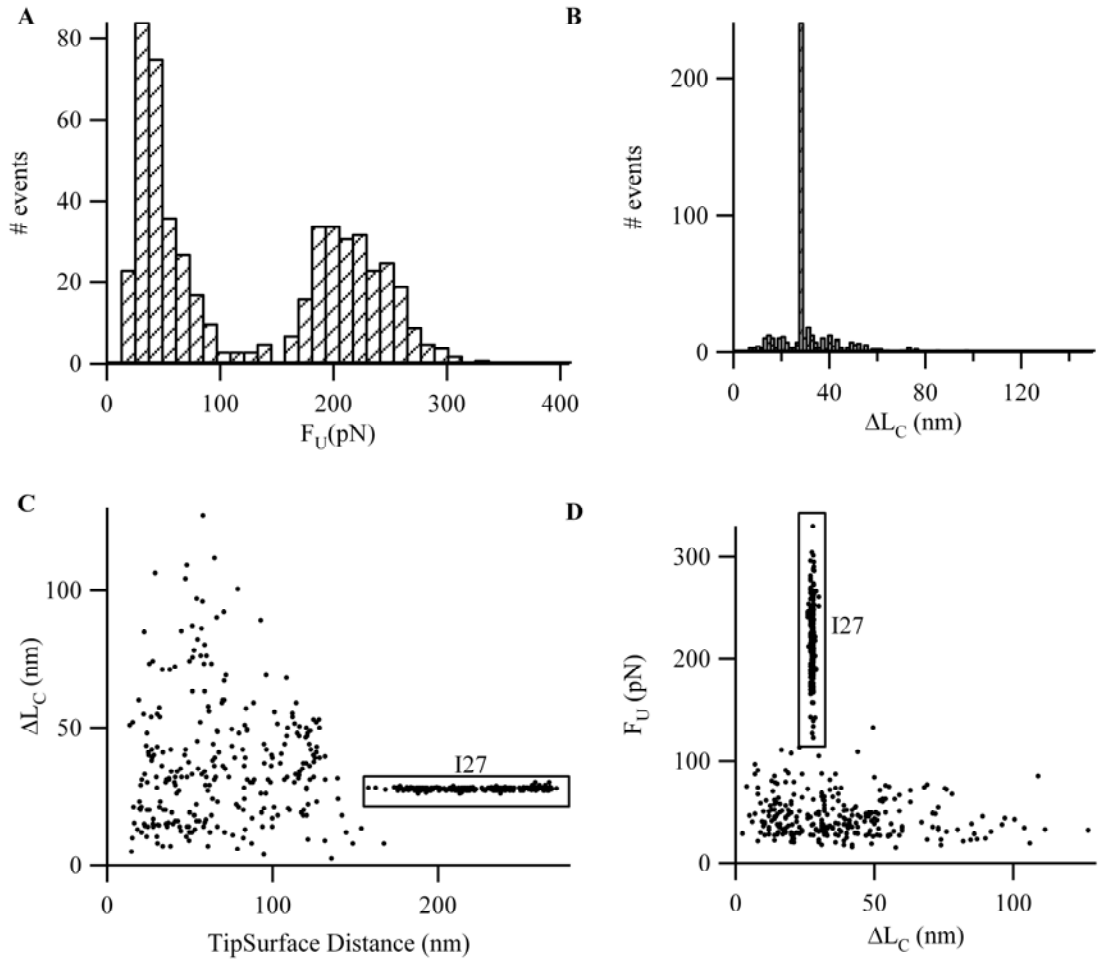
A
events
F_U(pN)
B
events
ΔL_C (nm)
C
ΔL_C (nm)
I27
TipSurface Distance (nm)
D
F_U (pN)
I27
ΔL_C (nm)

FIGURE S4

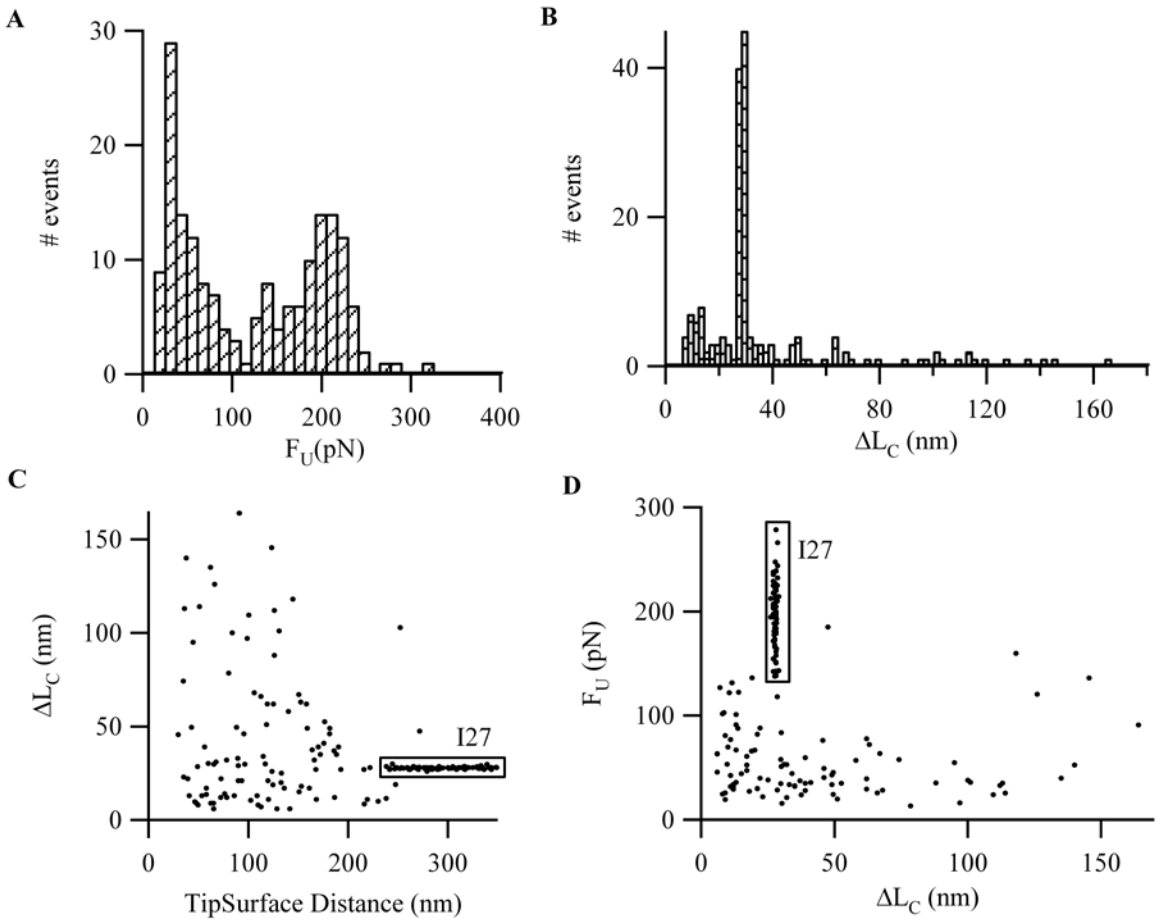
A
events
F_U(pN)
B
events
ΔL_C (nm)
C
ΔL_C (nm)
I27
TipSurface Distance (nm)
D
F_U (pN)
I27
ΔL_C (nm)

FIGURE S5

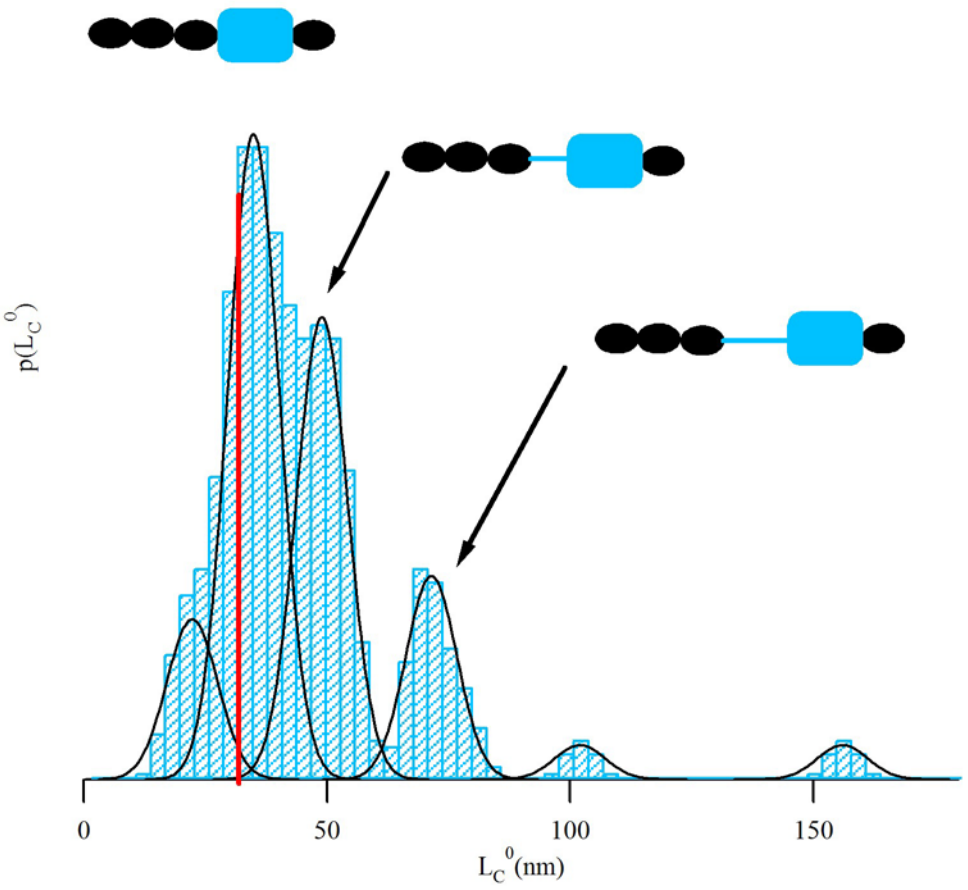

FIGURE S6

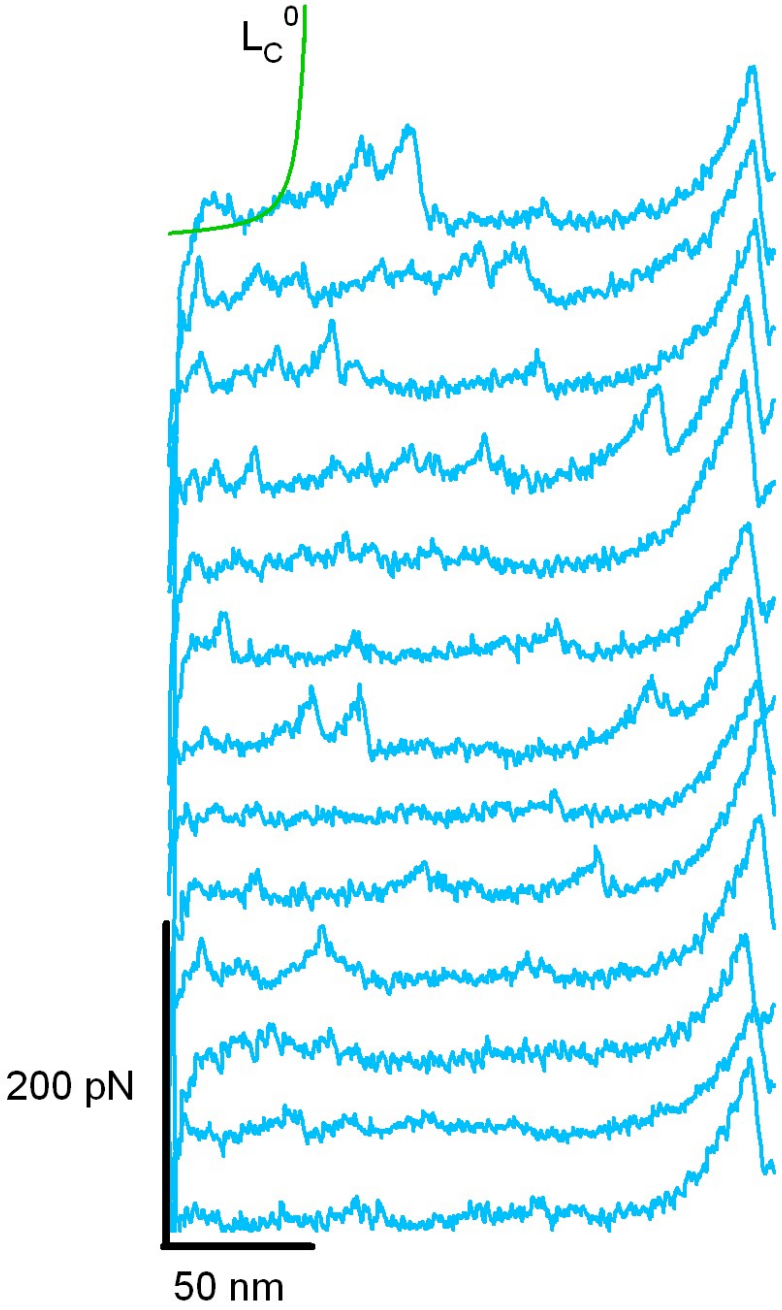

FIGURE S7

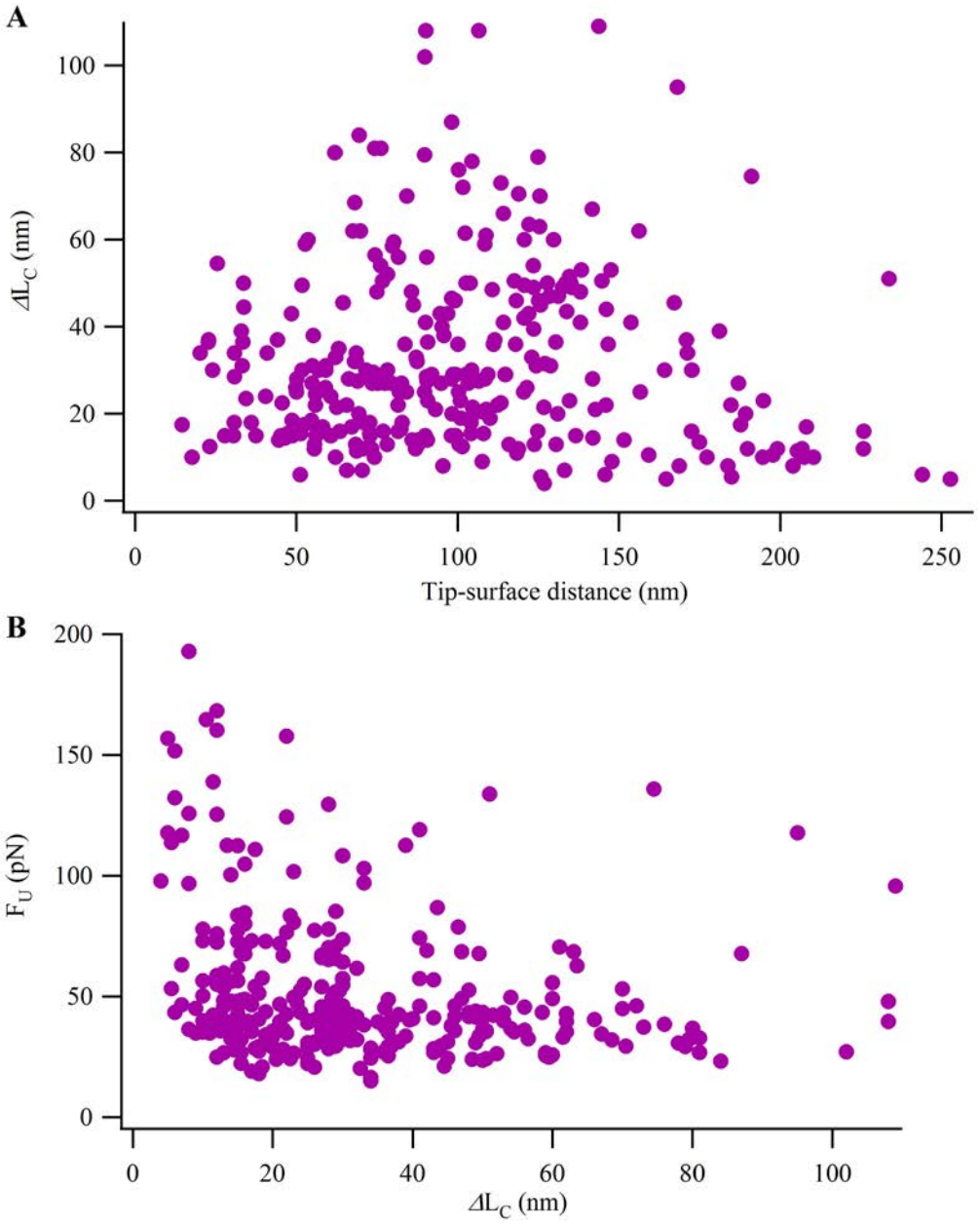
A
100
80
60
40
20
0
ΔL_C (nm)
0
50
100
150
200
250
Tip-surface distance (nm)
B
200
150
100
50
0
F_U (pN)
0
20
40
60
80
100
ΔL_C (nm)

FIGURE S8

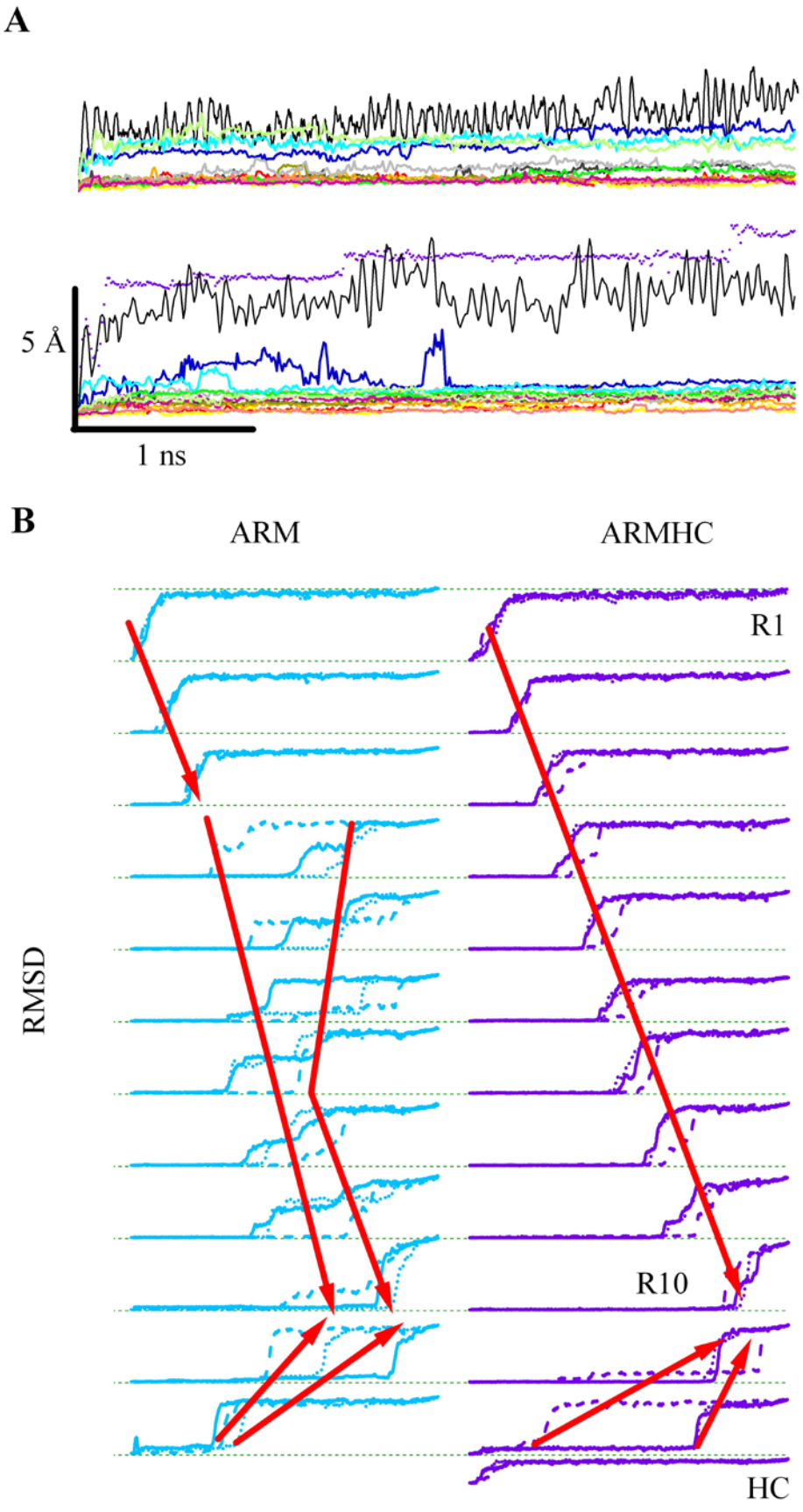

FIGURE S9

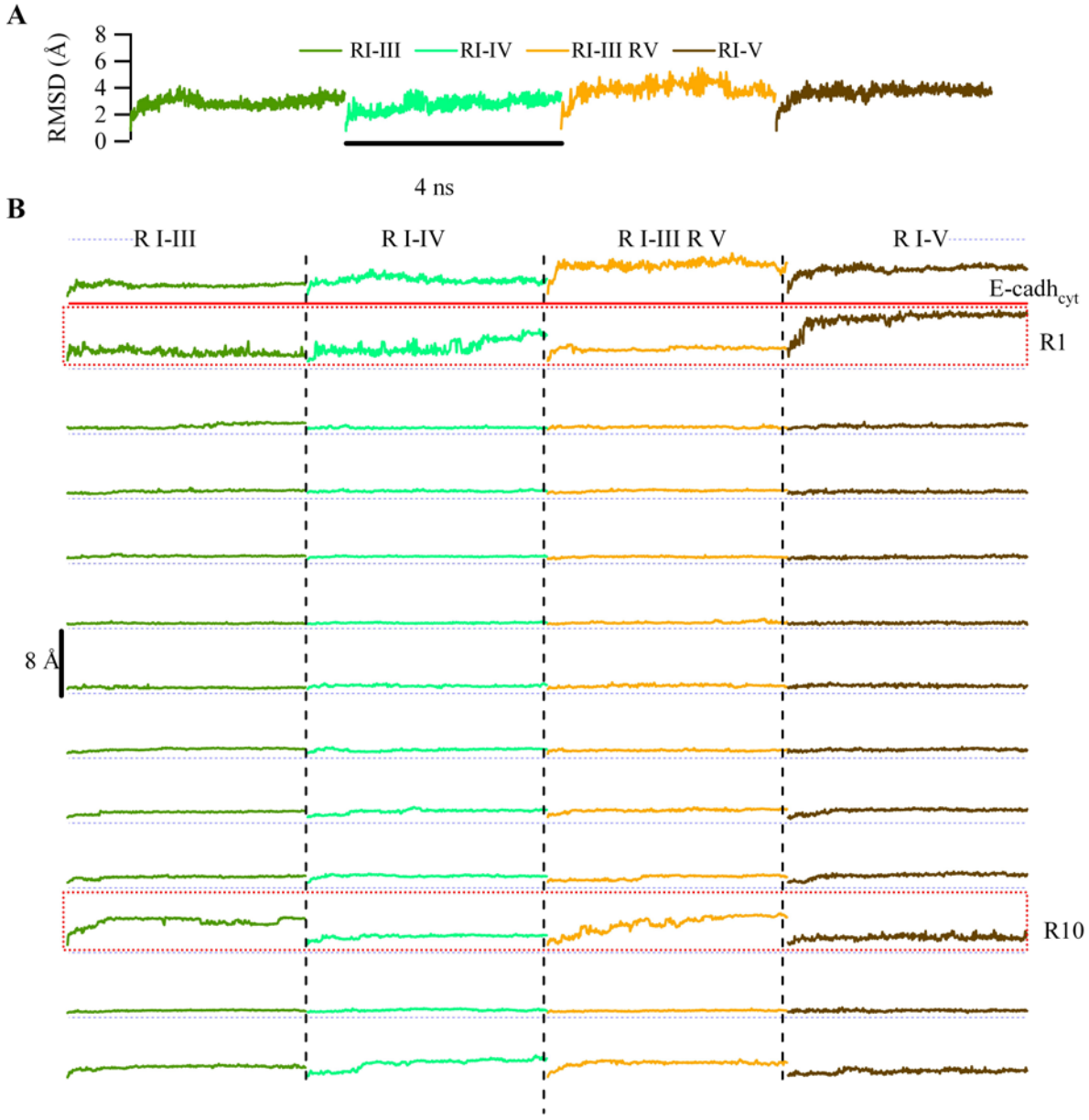
A
RMSD (Å)
8
6
4
2
0
RI-III
RI-IV
RI-III RV
RI-V
4 ns
B
R I-III
R I-IV
R I-III R V
R I-V
E-cadh$_{cyt}$
R1
8 Å
R10

FIGURE S10

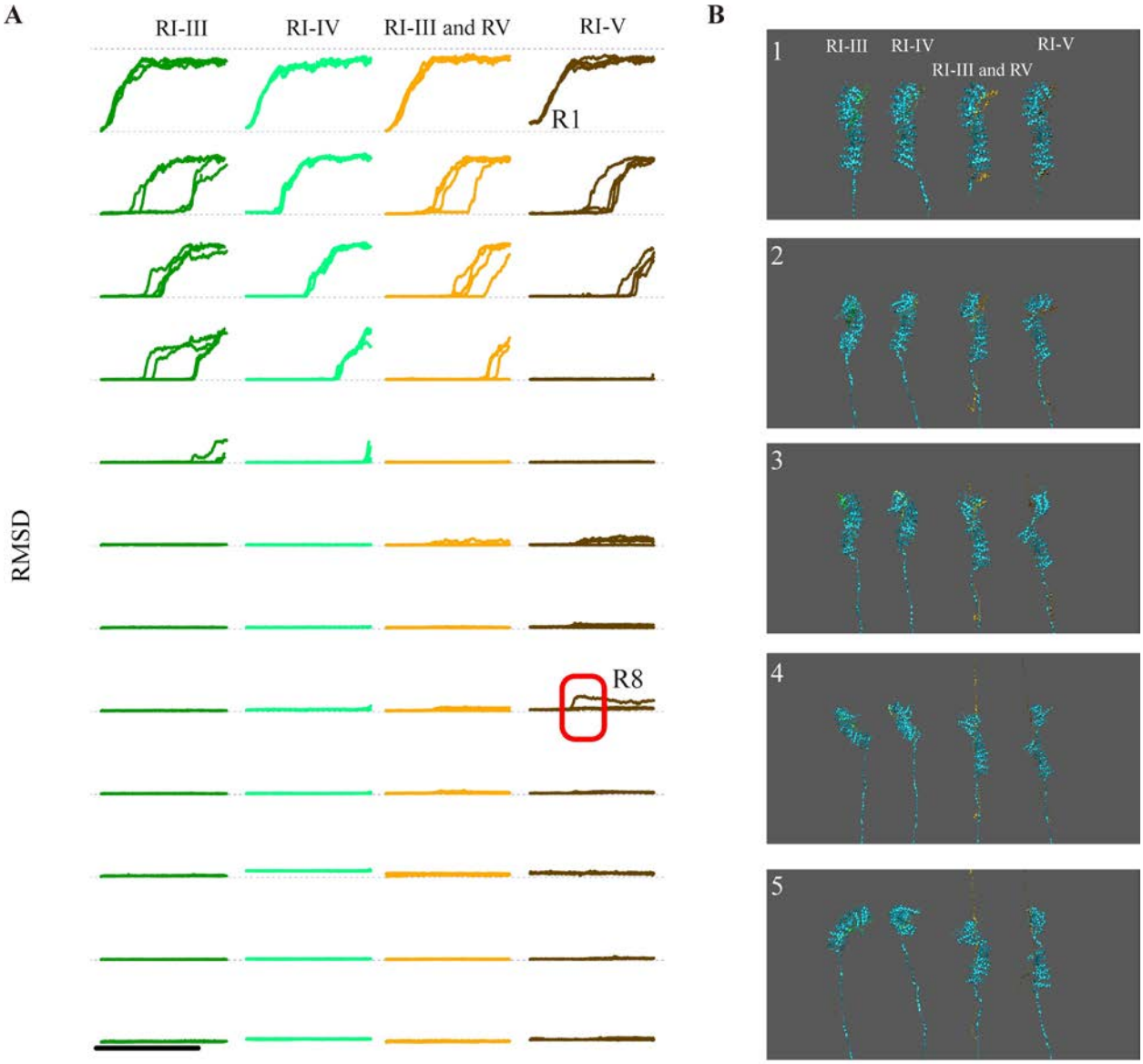
A
RI-III
RI-IV
RI-III and RV
RI-V
R1
R8
RMSD
B
1
RI-III
RI-IV
RI-III and RV
RI-V
2
3
4
5

FIGURE S11

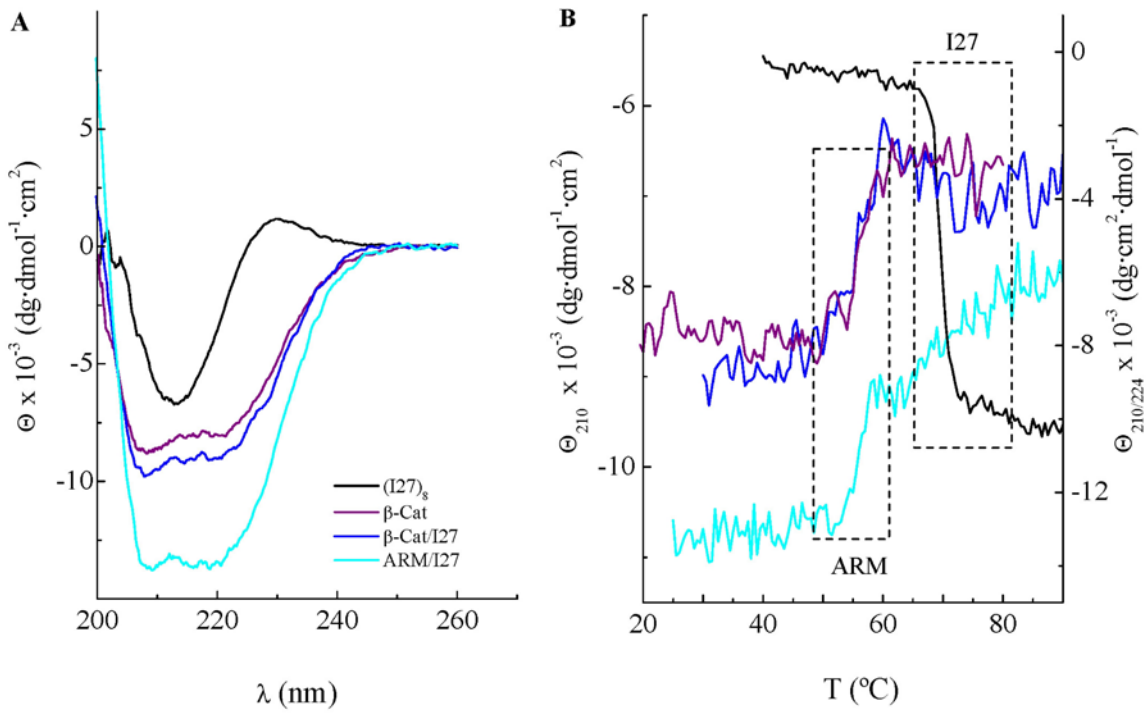
A
B
Θ x 10^-3 (dg·dmol^-1·cm^2)
λ (nm)
(I27)s
β-Cat
β-Cat/I27
ARM/I27
I27
ARM
Θ210 x 10^-3 (dg·dmol^-1·cm^2)
Θ210/224 x 10^-3 (dg·cm^2·dmol^-1)
T (°C)

LEGENDS TO SUPPORTING FIGURES

FIGURE S1 Structures used for the simulations of the ARM/cadherin complex. Detail of the structures used for the simulation of the stress applied to the ARM/cadherin complex. Different cadherin regions involved in the interaction were taken into account: RI-III (*A*), RI-IV (*B*), RI-III/RV (*C*) and RI-IV/RV (*D*). The color code used here will be maintained in **Figs. S9** and **S10**.

FIGURE S2 Effect of increasing the signal-to-noise ratio in our SMFS experiments and evidence for dynamic equilibrium of ARM repeat region (*A*) Comparison of the force noise distribution at 20 nm/s (brown histogram) and 400 nm/s (green histogram) of pulling speed. Reducing the pulling speed to 20 nm/s produced a decrease in the force noise of about 66% compared to that at 400 nm/s. **(*B*)** This particular trace was obtained at 20 nm/s. Apart from the noise reduction, recordings in both conditions were fully comparable. Indeed, at this lower pulling speed we were able to observe the unfolding of more than one ARM repeat simultaneously. **(*C*)** A graphical comparison of the force noise and the force unfolding histograms of ARMI27 (both at 400 nm/s) clearly shows minimal overlapping between both histograms, indicating that, even in "higher" noise conditions, the unfolding data were not significantly contaminated by noise.

FIGURE S3 Extracting the ARM region unfolding events from the ARMI27 recordings. (*A*) ARMI27 F_U histogram shows two discrete force distributions: low forces for the ARM region and forces around 200 pN for the I27 marker. The unfolding force distribution for I27 appears to be slanted at low values, presumably as an effect of the long linker constituted by the ARM region that always precedes the I27 unfolding events (S8, S9). **(*B*)** The ΔL_C histogram shows a high peak corresponding to the I27 marker embedded in multiple ARM unfolding events with variable ΔL_C values. **(*C*)** A scatter plot of the ΔL_C versus the tip-surface distance allows unfolding events from either the ARM region or the I27 modules to be identified. Thus, this graph permits filtering the crude data and extracting the ARM unfolding events. **(*D*)** A scatter plot of the F_U *vs*. ΔL_C shows the strong clustering of I27 ΔL_C values, in high contrast to those from the ARM repeats, suggesting that ARM unfolding goes through several alternative mechanical unfolding pathways, in contrast to that of I27 which seems highly canalized (25,43).

FIGURE S4 Extracting the β-catenin region unfolding events from the βI27 recordings. (*A*) Similarly to ARMI27, we can observe two discrete force distributions in the histogram of the F_U of the whole heteropolyprotein βI27: one corresponding to the β-catenin region with low forces, and another one for the I27 marker with forces around 200 pN. The distribution of F_U for I27 seems to be similar to that shown in **Fig. S3 *A***. **(*B*)** The histogram for the ΔL_C values is comparable to that seen in **Fig. S3 *B***, though with larger values due to the presence of the long disordered terminals. **(*C*)** The unfolding events from either β-catenin region or I27 modules can be identified based on a scatter plot of the ΔL_C *vs* the tip-surface distance. **(*D*)** By plotting F_U *vs*. ΔL_C we can identify the strongly clustered I27 values as opposed to those from β-catenin, suggesting alternative mechanical unfolding pathways for the latter.

FIGURE S5 Histograms of the length of the first force event (L_C^0) for ARMI27. Black lines are Gaussian fittings to all the distributions (see Material and Methods).

Solid red line indicates the length at which the force events arise from the ARM region unfolding. Some unfolding events lie above this line, meaning that some ARM repeats should be unfolded before they were stretched (indicated by the arrows and cartoon representations).

FIGURE S6 Variability in the mechanical unfolding pathway of the ARM region. In order to illustrate the diversity found in the mechanical unfolding of β-catenin, several unfolding force-extension traces of the ARM region are shown. The ARM unfolding traces showed force events variable in number, position, and ΔL_C, as opposed to the typical sawtooth pattern observed in most repeat-containing proteins studied (see I27 modules markers in **Fig 2 *A*).**

FIGURE S7 Full length β-catenin does not show any fixed mechanical unfolding pathway. Scattered plots of ΔL_C *vs.* tip-surface distance (***A***) and F_U *vs.* ΔL_C (***B***) show that this protein has not an ordered unfolding pathway, as also happened for the other two constructs analyzed in this study (**Figs. S3 *C*, S4 *C*, S3 *D*,** and **S4 *D***, respectively).

FIGURE S8 Monitoring single ARM repeats during free and steered MD (*A*) Backbone RMSDs for ARM (top) and ARMHC (bottom) during 4 ns of free MD. Each repeat is colored as follows: R1 blue, R2 red, R3 gray, R4 orange, R5 yellow, R6 olive, R7 light gray, R8 green, R9 pink, R10 cyan, R11 violet, R12 light green, helix C light blue (dotted line) and the whole structure in black. R1, R10 and R12 ARM repeats show lower deviation in the ARMHC structure. **(*B*)** Backbone RMSDs for ARM (left) and ARMHC (right) during the three trajectories (indicated as a continuous, broken or dotted lines). Red arrows indicate the order of the unfolding pathway and point to the last ARM repeat to unfold, illustrating to see the variability in the unfolding pathway. In the case of ARMHC, the unfolding pathway is almost the same in the three trajectories, suggesting a more "canalized" unfolding pathway.

FIGURE S9 RMSD of ARM/cadherin complexes during free MD (*A*) Backbone deviations for the entire ARM region in complex with the cadherin cytoplasmic tail. In the upper part we specify the different regions of cadherin that were considered. When RV is included in the structure, larger deviations are observed. **(*B*)** Individual RMSD for each ARM repeat and for the cadherin cytoplasmic tail. The cadherin cytoplasmic tail undergoes larger deviations when RV is included in the complex. It is interesting to note the larger deviations undergone by R10 ARM repeat (containing a longer loop, **Fig. S8 *A***) are decreased in the presence of the interacting region RIV.

FIGURE S10 Detail of ARM/cadherin complex stretching (*A*) Backbone RMSDs of each ARM repeat during the stretching of the complex. ARM repeats from R1 to R3 unfold later when all the interacting regions were included, suggesting a mechanical stabilization of these repeats. The small deviation observed in R8 after 25 nm of pulling corresponds to the conformational change observed between R8 and R9, leading to Tyr489 solvent exposure. **(*B*)** Different snapshots of the mechanical stretching of the complex. RI-V refers to RI-IV/V in the main text.

FIGURE S11 Circular Dichroism analysis of the fusion proteins (*A*) Far-UV CD spectra of ARMI27, βI27, β-catenin and $(I27)_8$. The spectra indicate that β-catenin maintains its typical fold when fused to I27. Colors are maintained in the rest of the figure. **(*B*)** Thermal denaturation of ARMI27, βI27, β-catenin and $(I27)_8$. CD transitions

were monitored following the ellipticity (Θ) changes at 210 nm (ARMI27, βI27 and β-catenin) and 224 nm ($(I27)_8$) as a function of temperature. Interestingly, heteropolyproteins show two transitions in their thermal denaturation. Estimated half transition temperatures ($T_{1/2}$) were: ARMI27 ($T^1_{1/2}$ ~ 55.9 ºC; $T^2_{1/2}$ ~ 65.4 ºC); βI27 ($T^1_{1/2}$ ~ 55.7 ºC; $T^2_{1/2}$ ~ 67.8 ºC); β-catenin ($T_{1/2}$ = 56.1 ± 0.4 ºC) and $(I27)_8$ ($T_{1/2}$ = 69.2 ± 0.1 ºC). Dotted line boxes indicate the transition regions for ARM and for I27 modules.